Controlling the Degree of Crystallinity and Preferred Crystallographic Orientation in Poly-Perfluorodecylacrylate Thin Films by Initiated Chemical Vapor Deposition

*Anna Maria Coclite, Yujun Shi, and Karen K. Gleason**

Preferred crystallographic orientation (texture) in thin films of technologically important materials frequently has a strong effect on the properties of these films and is important for stable surface properties. The deposition of organized molecular films of a poly-perfluorodecylacrylate, poly-(1*H*,1*H*,2*H*,2*H*-perfluorodecyl acrylate) (p-PFDA), by initiated chemical vapor deposition (iCVD) is described. The tendency of p-PFDA to crystallize in a smectic B phase has been reported in films prepared from solution but not for those using a CVD technique. The degree of crystallinity and the preferred orientation of the perfluoro side chains, either parallel or perpendicular to the surface, are controlled by tuning the CVD process parameters (i.e., initiator to monomer flow rate ratio, filament temperature, and substrate temperature). Films with no observable X-ray diffraction patterns are also achieved. The observed differences in crystal texture strongly impact the observed water contact angles (150° to 130°, advancing) and corresponding hysteresis behavior. Low hysteresis (<7°) is associated with high crystallinity, particularly when the orientation of the crystallites resulted in the perfluoro side groups being oriented parallel to the surface. The latter texture resulted in smoother film than the texture with the chains oriented perpendicular to the surface and this can be very advantageous for applications in which relatively smooth but still crystalline films are needed.

1. Introduction

Low-surface-energy surfaces with hydrophobic and oleophobic characteristics are highly desirable for various applications including biocompatible surfaces,[1,2] antifouling coatings,[3] and low dielectric constant material for microelectronics.[4]

Recently, much attention has been paid to produce low-surface-energy fluorocarbon polymer coatings of perfluoroacrylates due to their exceptional properties, such as fast polymerization of the unsaturated acrylate group and therefore requirement of mild processing conditions[5,6] and hydrophobicity due to the fluorinated pendant groups as well as excellent chemical and thermal stability.[7] When enough fluorine is present in one of the pendant groups, the side chains organize in such a way that very hydrophobic and oleophobic properties appear. In the literature, it is shown that $-(CF_2)_nCF_3$ chains longer than eight units ($n \geq 7$) in poly-perfluoroacrylates form aggregates in an ordered lamellar structure called smectic B phase.[7,8] The smectic B structure with a periodicity of 32.4 Å of poly-(1*H*,1*H*,2*H*,2*H*-perfluorodecyl acrylate) (p-PFDA) is shown in **Scheme 1**. The smetic B structure consists of a succession of bilayers of pendant perfluorinated groups coming alternatively from two different polymer chains. The axes of the side perfluorinated chains are perpendicular to the plane of the hexagonal lamellar packing with a lattice parameter of 6.4 Å.[9] In particular, thin p-PFDA films have also shown a preferred crystallographic orientation[9] that can be associated with a fiber texture: one crystallographic axis of the film is parallel to the substrate normal, while there is a rotational degree of freedom around the fiber axis.

Important materials properties, such as remanent polarization, the dielectric constant, and the elastic moduli, are typically anisotropic and the most effective use of anisotropic materials in thin film applications often involves controlling the texture of the films.[10] Pittman and Ludwig[11] were the first to demonstrate that the wetting properties of polymers containing fluorinated side chains can be markedly influenced by packing of the side chains resulting from crystallization. Polymers containing crystalline segments involving fluoroalkyl side chains can lead to surface tension values lower than the values obtained for amorphous polymers. The lower critical surface tension of many polymers with fluorinated side chains reflects a high concentration of CF_3 groups on the surface. Milella et al.[12] obtained a superhydrophobic coating with ribbon-like structure by pulsed plasma enhanced chemical vapor deposition (PECVD). They demonstrated that the ribbon-like features were composed of semicrystalline chains of CF_2 groups terminating with CF_3.

Dr. A. M. Coclite, Prof. K. K. Gleason
Department of Chemical Engineering
Massachusetts Institute of Technology
Cambridge, MA 02139, USA
E-mail: kkg@mit.edu
Prof. Y. J. Shi
Department of Chemistry
University of Calgary
Calgary, Alberta, Canada

DOI: 10.1002/adfm.201103035

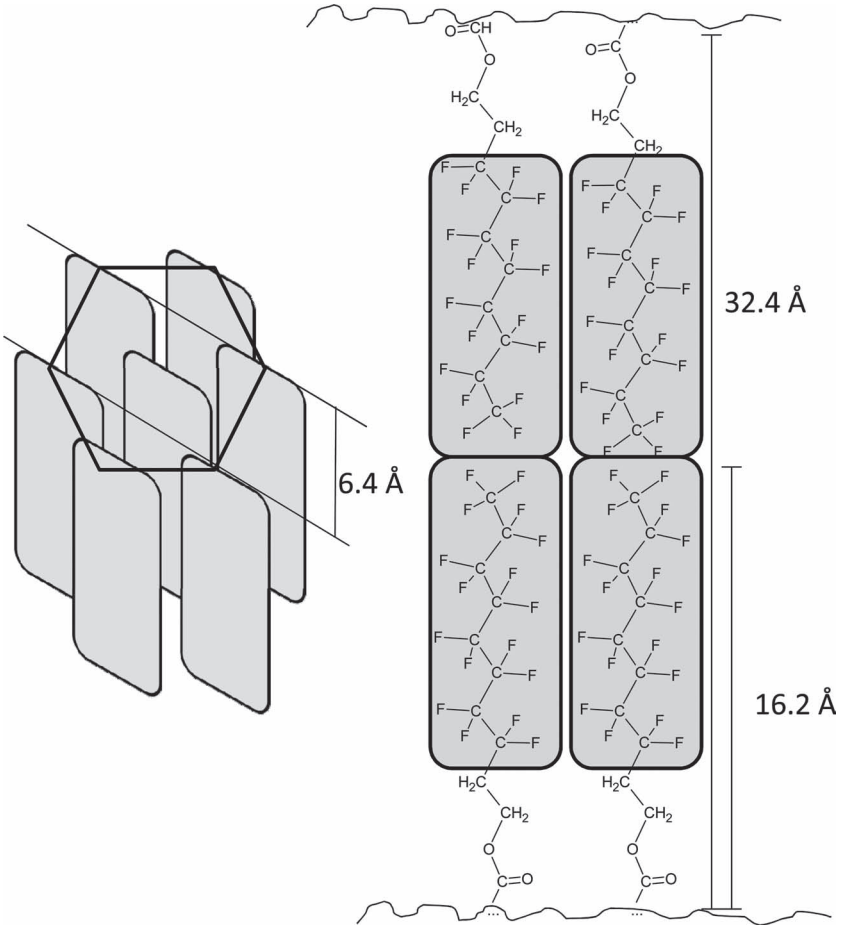

Scheme 1. Smectic B structure with a periodicity of 32.4 Å of p-PFDA. The smetic B structure consists of a succession of bilayers of pendant perfluorinated groups coming alternatively from two different polymer chains. The axes of the side perfluorinated chains are perpendicular to the plane of hexagonal lamellar packing with a lattice parameter of 6.4 Å.

The aim of the present work was to demonstrate if and under which conditions it is possible to obtain a semicrystalline polymer of PFDA by initiated chemical vapor deposition (iCVD). Vapor deposition eliminates the need to use costly fluorinated solvents. The iCVD technique is based on the thermal decomposition of an initiator (generally a peroxide), in order to create primary radicals.[13,14] The decomposition takes place in the gas phase and it is driven by a filament heated to 250–300 °C. Temperatures in this range are able to break only the labile peroxide bond of the initiator molecule, while the monomer is not decomposed.[5] The initiator radicals then attack the vinyl bond of the monomer, creating heavy I–M* fragments that are adsorbed on the substrate, which is cooled in order to promote the adsorption. The chain growth and polymerization reactions (resulting in I–M_n polymers) then take place on the substrate. The free radical mechanism indeed results in limited incorporation of the initiating fragments in the deposited film, but the degree of initiator fragment incorporation is difficult to determine from Fourier transform infrared (FTIR) spectroscopy, suggesting that it is ≈1% or less, consistent with the initiator fragments being the endgroups for polymer chains of reasonable length. The low-molecular-weight initiator fragments are expected to have a high volatility (i.e., a high vapor pressure) and thus have a limited degree of absorption on the surface.

The advantage of using iCVD over other vapor deposition techniques, (e.g., PECVD or physical vapor deposition) is the ability to control the possible reaction pathways and thus fully retain the functional groups of the monomer without the breaking and recombination of dangling bonds due to plasma ion bombardment or to precursor pyrolysis. The long fluorochain of the PFDA monomer (–$(CF_2)_7CF_3$) has been already demonstrated to be completely preserved after the iCVD polymerization steps,[5] while no attention has been devoted to the investigation of the molecular aggregation that can be achieved with the p-PFDA coatings deposited by iCVD. Another aspect that makes the molecular aggregation achievable by iCVD is that it has been largely demonstrated that the deposition conditions determine transitions in kinetic regimes[15] as well as differences in the species initiating the polymerization and this affects important coating properties (i.e., the deposition conformality).[16] Therefore it is expected that the deposition conditions would play an important role in determining the crystallinity of the p-PFDA thin films as well. In particular, we studied the effect of the initiator flow rate, filament temperature, and substrate temperature (**Scheme 2** shows the process schematic for iCVD indicating the variables that will be varied in this study) on the molecular organization and on the film properties, such as dynamic water repellency and surface morphology.

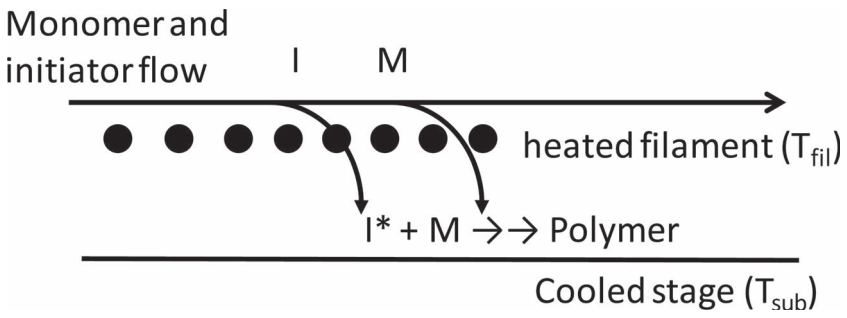

Scheme 2. Schematic of the iCVD process indicating the different variables that are varied in this study.

Table 1. Deposition conditions used for the growth of p-PFDA thin films by iCVD.

Experiment set	PFDA flow rate [sccm]	TBPO flow rate [sccm]	N_2 flow rate [sccm]	I/M	Pressure [mTorr]	T_{fil} [°C]	T_{sub} [°C]
set I/M	0.6	0.3–3.6	4.3–1	0.5–6	200	250	30
set T_{fil}	0.2	0.4	–	2	200	240–300	40
set T_{sub}	0.6	1.2	3.4	2	200	250	20–50

2. Results and Discussion

The iCVD technique has been used to create low-surface-energy p-PFDA thin films at high deposition rates (higher than 100 nm min^{-1}).[5] FTIR spectroscopy and X-ray photoelectron spectroscopy (XPS) showed full retention of the fluorine moieties and no measurable cross-linking. Gel permeation chromatography showed that the iCVD p-PFDA films have molecular weight values ranging from 42.8 to 177.3 K with polydispersity index ranging from 1.89 to 2.63.

The same chemical composition was reproduced in this study using the deposition conditions reported in **Table 1**. As reported in Supporting Information Figure 1, the spectra of the p-PFDA are comparable with those reported in the literature.[5] The XPS C/F and C/O elemental ratio calculated from the polymer are largely comparable to those calculated considering the monomer formula: C/F is 0.71 in the polymer and 0.76 in the monomer, and the C/O ratio is 0.11 in the polymer while in the monomer it is 0.12, meaning that the monomer structure was fully retained upon polymerization. No significant differences were found in the chemical composition of the polymer samples when changing the deposition conditions, which indicates that varying the iCVD polymerization conditions does not change the local chemical bonding environment in the polymers.

2.1. Initiator to Monomer Flow Rate Ratio

The ratio of initiator flow rate to the monomer flow rate (I/M) during the iCVD growth was found to be one of the most significant variables for controlling the structure and properties of the resultant p-PFDA films. This section describes the observed systematic changes in the crystallinity index (CI), deposition kinetics, water contact angle (WCA) hysteresis, and surface morphology with increasing I/M.

Figure 1 shows the X-ray diffraction (XRD) 2θ–θ scans of the coatings deposited at different flow rate ratio of initiator to monomer (I/M). All the peaks are in the small-angle region ($\theta < 10°$), precisely at $\theta = 2.8°$, 5.6°, and 8.3° (corresponding to spacing $d = 32.4$, 16.2, 10.8 Å). These peaks are assignable to successive diffraction orders characteristic of the bilayer structure: 32.4 Å is exactly the length of the double layer and 16.2 Å corresponds to the length of one single chain as reported in Scheme 1. The double perfluorinated chains do not interpenetrate, probably due to the large size and the rigidity of the pendant groups. In the pattern in Figure 1, the peak at $\theta = 13.8°$ ($d = 6.4$ Å), which is characteristic of the hexagonal packing of the fluorochains, is not distinguishable while it is evident when measuring the XRD from p-PFDA powder in which the crystals are randomly oriented.[7] The absence of the peak at 13.8°, corresponding to the plane (100), the crystallographic plane that is parallel to the substrate, indicates that the p-PFDA coatings deposited by iCVD show a preferred orientation: the lamellar structure is oriented parallel to the substrate with the fluorinated groups oriented almost perpendicular to the substrate. This organization can be assimilated to a fiber texture.

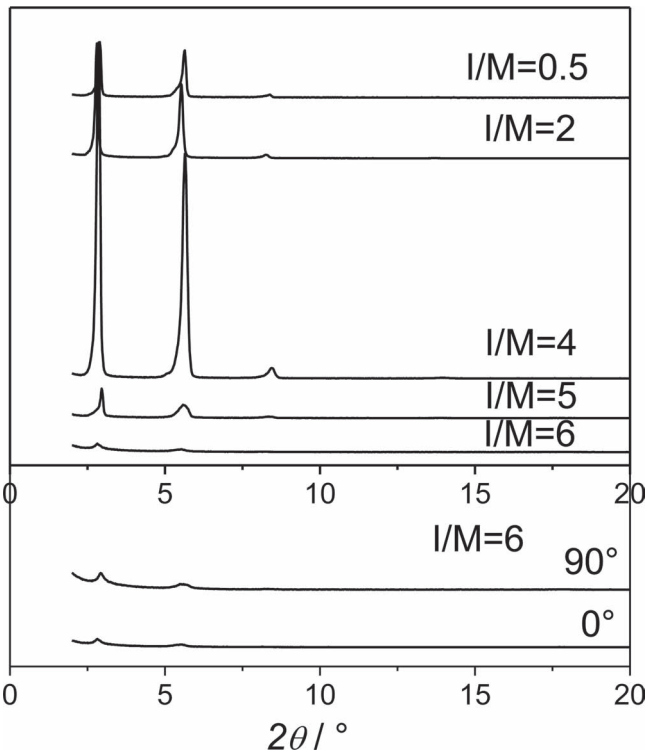

Figure 1. Top: XRD with the beam incident along the substrate surface normal (0°) for iCVD p-PFDA deposited at different ratios of the initiator to monomer (I/M) flow rates. Bottom: For the sample with I/M = 6, the XRD at beam angles of 0° and 90°. All the spectra were normalized to the sample thickness. The sample deposited at I/M < 5 shows a very definite diffraction pattern characteristic of a semicrystalline phase.

At low I/M values the XRD peaks are sharp and at I/M = 4 the peak intensity reaches a maximum. At even higher I/M values, the diffraction peaks broaden. For the case of I/M = 6, very broad diffraction patterns are detected both orienting the beam at 0 and 90° with respect to the surface normal (as shown in **Scheme 3**). Thus, at high I/M ratio a transition from a semicrystalline to an amorphous phase occurs. At high I/M, a great number of tert-butoxy radicals are created from the thermal fragmentation of the initiator. These bulky radicals can be incorporated as endgroups during chain initiation and termination. We hypothesize that these large endgroups disorder the lamellar structure of p-PFDA. Corpart et al.[11] studied the role of the spacer groups located in the side chain of fluoropolymers and they also observed that when the steric hindrance of the spacer group is too high the polymers are amorphous.

Figure 2 shows how the transition from the semicrystalline to the amorphous phase affects the deposition kinetics and

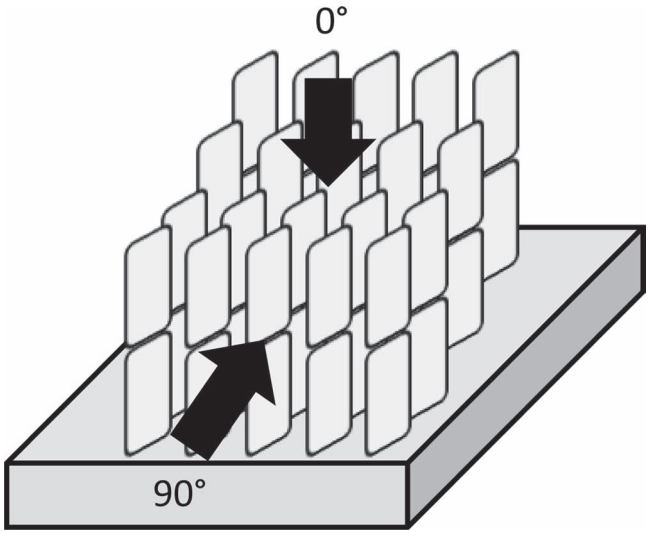

Scheme 3. Different orientations of the X-ray beam (0 and 90° with respect to the surface normal) used for the XRD investigation.

the surface properties. In Figure 2a the crystalline index (CI) or relative intensity of the XRD crystalline contribution to the peak centered at 2.8° is reported as a function of the I/M ratio. On the right axis of the same figure the deposition rates are plotted. In semicrystalline material, the crystalline peaks generally superimpose on an amorphous contribution due to the scattering from the amorphous domains. For this reason, it is generally preferred to deal with relative intensities rather than with absolute intensities. The classical procedure to calculate the CI consists of evaluating the ratio of the areas of the crystalline peaks (I_c) to the total area under the scattering curve.[17]

$$\mathrm{CI} = \frac{I_c}{I_c + I_a} \quad (1)$$

where I_a is the area due to the scattering from the amorphous domains. In the case of the p-PFDA the crystalline peaks are well resolved and therefore the scan can be fitted with an amorphous halo and crystalline peaks reliably, without imposing any special constraints in the least-squares procedure. The least-squares regression of the XRD signals at 2.8° was obtained with two Lorentz components at 2.85 and 2.8° (as reported in the Supporting Information Figure 2).

As shown in Figure 2 the CI reaches a maximum of 0.75 for the sample deposited at I/M = 4. At these conditions the deposition rate is relatively low, ≈30 nm min^{-1}. In a previous study, partial crystalline coatings were obtained by PECVD after 90 min of treatment while in this case the deposition was only 10 min long and the diffraction pattern for the PECVD sample was not as sharp as the one reported in this study.[12] Increasing the initiator flow rate up to I/M = 6 substantially lowers the CI while improving the deposition rate to ≈170 nm min^{-1}. The trend of the deposition rate varying the initiator flow rate is substantially different from what has been previously observed: published studies of iCVD show a monotonic increase in the deposition rate as I/M increases up to a point, followed by a plateau or decrease in rate.[18–20] We hypothesize that the presence of crystallinity in p-PFDA is the differentiating factor in

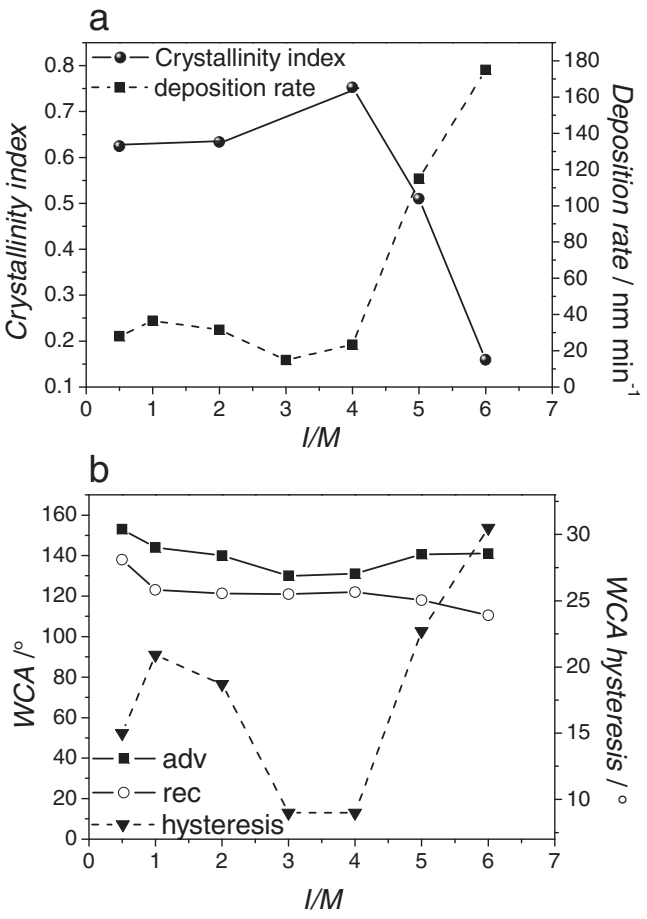

Figure 2. a) CI and deposition rate reported as a function of the I/M ratio. The CI was calculated as the area of the crystalline peak at 2.8° divided by the total area under the scattering curve. The formation of a crystalline phase decreases the polymer growth rate. b) Advancing and receding WCAs as a function of the I/M ratio. On the right axis of (b) the hysteresis is reported; it was calculated as the difference between the advancing and the receding WCAs. For I/M between 3 and 4, the CI is maximum while the WCA hysteresis is minimum.

the current iCVD kinetic study. Specifically, the smectic B phase seems to suppress the deposition rate achievable at I/M ≤ 4, while p-PFDA films with a higher amorphous fraction deposit quite rapidly.

The degree of crystallinity is also hypothesized to impact the observed dynamic water contact angles (WCA), advancing and receding, and the hysteresis calculated as the difference between them. Figure 2 shows that increasing I/M ratios, the advancing WCAs decrease from 150° to 140° while receding WCAs remain constant (120°) and then decrease at I/M > 4. This change in hysteresis behavior is quite significant and can result from changes in the surface roughness, chemical composition heterogeneities, reorientation, and mobility.[21,22] At high I/M, where the amorphous fraction is highest, the hysteresis is higher than 20°. When I/M is around 3–4, where the crystallinity is highest, the hysteresis reaches a minimum of 9–10°. We hypothesize that crystallinity is responsible for hindering

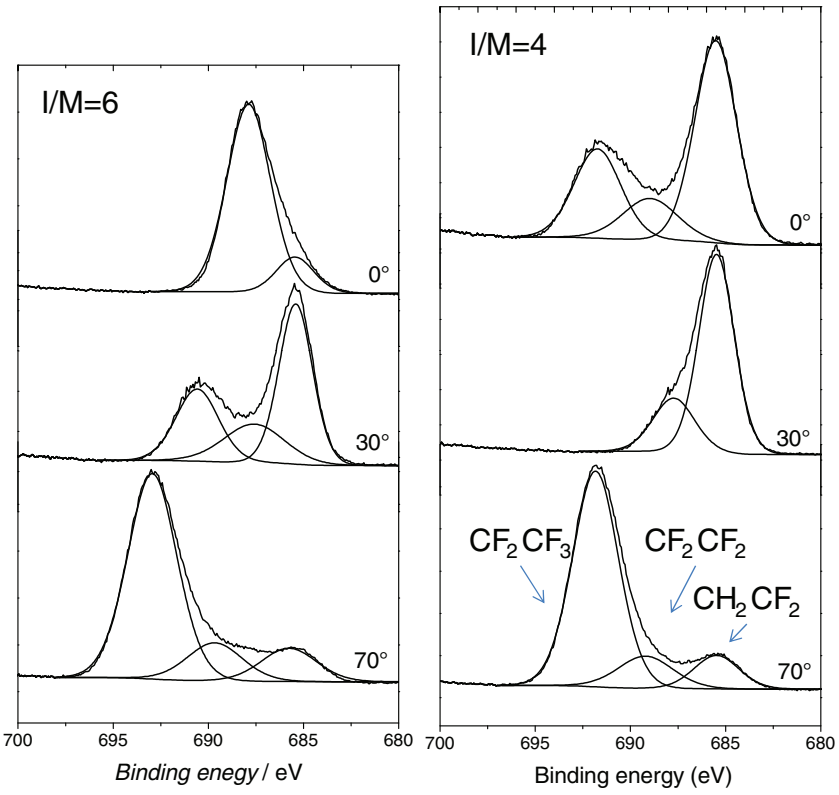

Figure 3. Angle-resolved high-resolution F1s XPS at take off angles of 0°, 30°, and 70°, corresponding to penetration depths of approximately 7, 6, and 2.5 nm, respectively. Right: In an amorphous film (I/M = 6), the observation of CF_3 (693 eV binding energy, BE) only at 70° incidence demonstrates the strong surface segregation of the CF_2CF_3. This is evidence of sufficient chain mobility to produce reorganization at the surface. Left: At high crystallinity (I/M = 4), the CF_3 can also be observed at a 0° take-off angle in depth, demonstrating reduced surface reorganization when crystallinity is present.

the mobility of p-PFDA chains, hence reducing the degree of surface rearrangement when exposed to water.[7]

The surface structure of the p-PFDA was also evaluated using angle-resolved XPS (ARXPS). **Figure 3** shows the angle-resolved high-resolution scans of the F1s XPS peak for the samples deposited at I/M = 6 and 4 at the take-off angles of 0°, 30°, and 70° with respect to the surface normal. Lower take-off angles correspond to higher penetration depth. In particular at 690 eV, 0° corresponds to ≈7 nm, 30° to 6 nm, and 70° to about 2.5 nm. The penetration depths were estimated using an inelastic mean free path (IMFP) of 2.4 nm because most of the polymers have an IMFP in the range 2.6–2.3 nm at 700 eV.[23] The F1s peaks were resolved with three components at 685.5 eV, 689.7 eV, and 691.6 eV and they can be assigned to different fluorine environments CH_2CF_2, CF_2CF_2 (similarly to polyperfluoroethylene, PFTE), and CF_2CF_3, respectively.[24] The least squares regression was obtained fixing the full width at half-maximum (FWHM) at 2–3 eV. The XPS Scienta Database shows F1s peaks with a FWHM of 2 eV. Therefore the range 2–3 eV was chosen, also taking into account the broadening created by the 1 eV electron beam used to compensate the charge during the analysis. The CF_3 component of the F1s peak increases in intensity at higher take-off angle. The ability of CF_3 groups to concentrate at the surface is a consequence of the higher chain mobility of the amorphous component: the most hydrophobic component moves toward the surface in order to reduce the energy at the film's interface with the air.[25] This surface reorganization becomes less prevalent as crystallinity increases. At I/M = 4, which has the highest CI, a strong CF_2CF_3 component is detected in depth, resulting from the higher rigidity of the chains in the semicrystalline structure and further confirming the lower degree of surface reorganization. The presence of the CF_3 component in depth for the sample deposited at I/M = 4 can be appreciated also in the XPS C1s peak (as reported in the Supporting Information Figure 3). Additionally, Schmidt et al.[26] found a minimum C/F ratio at 6 nm below the surface and then an increase at 8 nm. They ascribed this to the perfluoroalkyl layered structure.

Furthermore, the surface morphology is not the dominant factor in the WCA hysteresis behavior of iCVD p-PFDA. Generally, a higher surface roughness enhances the hysteresis.[27,28] We observe, instead, the exact opposite: amorphous films show smoother surfaces and the highest dynamic water repellency. The root-mean-square (RMS) roughness measured by atomic force microscopy (AFM) decreases from 40 to 10 nm as I/M increases from 0.5 to 6.0. Thus, the most important factor affecting the dynamic water repellency is the difference in chain mobility between the semicrystalline and amorphous states rather than the change in surface morphology.

Figure 4 shows the AFM images of iCVD p-PFDA films deposited at I/M = 0.5, 4, and 6. The tapping-mode phase imaging (Figure 4, left) is reported together with the topographical mapping (Figure 4, right) because it can be useful to detect variations in composition, adhesion, friction, viscoelasticity, and other properties. These AFM images show the presence of island growth. It is expected that island density at the surface of the film is controlled by the combination of: i) nucleation rate, which is expected to increase with I/M, and ii) overall film thickness. The film thickness was fixed at 300 nm for all the three samples. At I/M = 0.5 (Figure 4a,b) we measured the maximum RMS roughness (40 nm) and the surface is characterized by high density of small islands. As the I/M ratio increases, the islands decrease in density but increase in size, indicating that the islands probably coalesce into larger ones. The morphology of the sample deposited at I/M = 4 (Figure 4c,d) appears to be made of islands with non-rounded edge features, also evident in the phase image, with a diameter ranging from 100 to 200 nm and a maximum height of 100 nm. We hypothesis that this distinct island morphology is driven by faceting resulting from the high degree of crystallinity under these conditions. Finally, the islands detected on the surface of the sample deposited at I/M = 6 have a large diameter (≈500 nm) but do not produce a corresponding increase in surface roughness. These larger islands have rounded edges, consistent with a higher amorphous content.

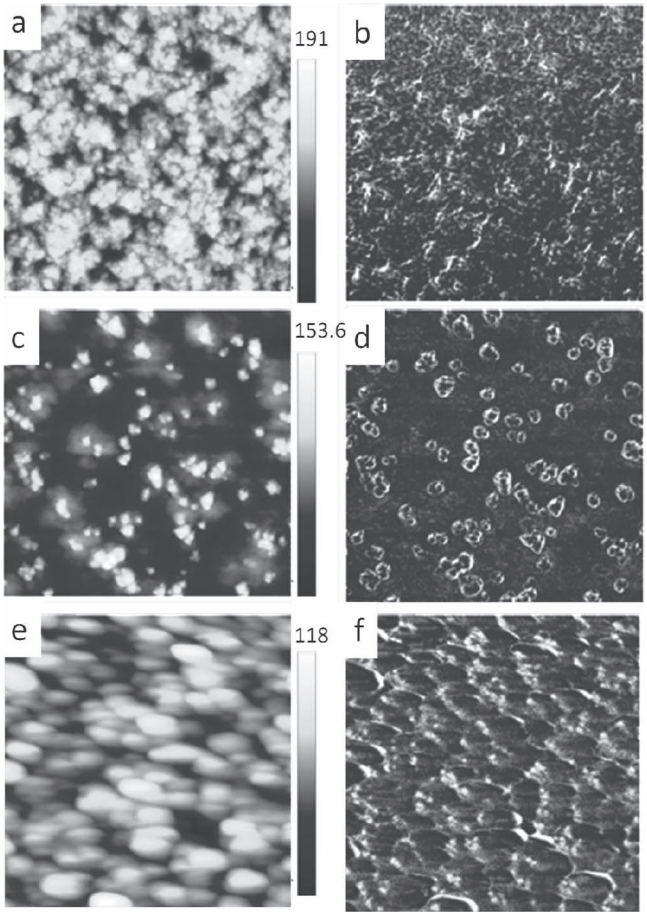

Figure 4. Topographical (a,c,e) and phase (b,d,f) AFM images for the samples deposited at I/M = 0.5 (a,b), I/M = 4 (c,d), and I/M = 6 (e,f). The lateral scale for all the images is 5 μm × 5 μm. The phase image for the sample deposited at I/M = 4 is evidence for the formation of islands that can be crystalline domain clusters. The sizes of the domains range from 100 to 200 nm.

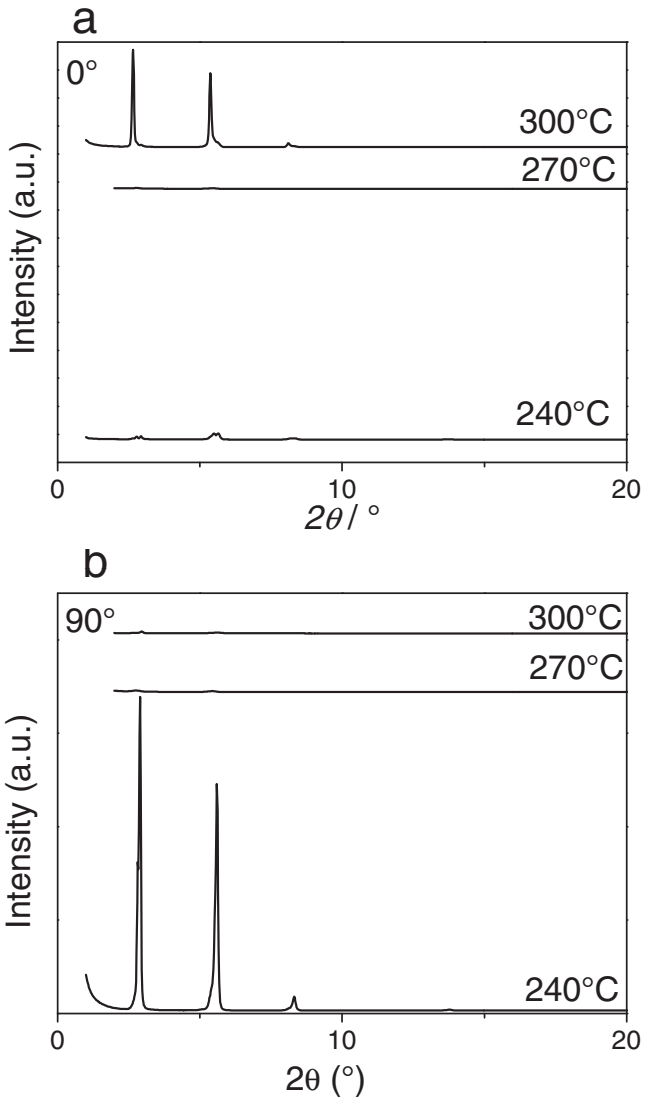

Figure 5. XRD profiles for the coating deposited at different filament temperatures. When the samples are oriented perpendicularly to the beam (0°) the XRD peaks sharpen at higher *T*. The contrary applies when the samples are oriented parallel to the beam (90°).

2.2. Filament Temperature

Another factor that may greatly influence the molecular organization of the p-PFDA polymers is the filament temperature, T_{fil}. In the range of T_{fil} used, 250 to 300 °C, the PFDA monomer should experience little, if any, degradation.[5] However, T_{fil} has a strong influence on the decomposition of tert-butyl peroxide (TBPO) initiator.[15] For T_{fil} < 270 °C, the cleavage of the peroxide linkage in the TBPO yields tert-butoxy radicals as the primary decomposition product, with the degree of decomposition increasing as T_{fil} increases. At higher T_{fil}, β-scission reactions of the tert-butoxy radicals occur, producing methyl radicals.[29]

Figure 5 shows the crystal texture of iCVD p-PFDA coatings deposited at different filament temperatures by means of XRD patterns taken at irradiation angles of 0° (Figure 5a) and 90° (Figure 5b) with respect to the surface normal. For T_{fil} = 300 °C, sharp intense diffraction peaks corresponding to intermolecular spacings of 32.4, 16.2, and 10.8 Å are observed for the perpendicular beam orientation (0°, Figure 5a). In contrast, in the parallel beam orientation (90°, Figure 5b), no diffraction peaks are observable for the T_{fil} = 300 °C sample. This phenomenon can be indicative of a bilayer structure with fiber texture in which the perfluoro side groups are oriented perpendicular to the surface of the substrate (**Scheme 4**b).

For the T_{fil} = 240 °C sample, similar diffraction peaks are observed, however, surprisingly, the intensity is strongest in the parallel beam orientation (90°, Figure 5b). The predominate structure in this case seems to be switched to the one with the perfluoro side groups parallel to the surface of the substrate (Scheme 4a). The sample deposited at T_{fil} = 270 °C did not show any diffraction pattern at either 0° or 90°; apparently when switching from one texture to another the polymer goes through a stage in which the chains are disordered and therefore the amorphous component seems to dominate.

Although measuring the diffraction pattern at only two angles (0° and 90°) cannot be considered a full texture analysis,

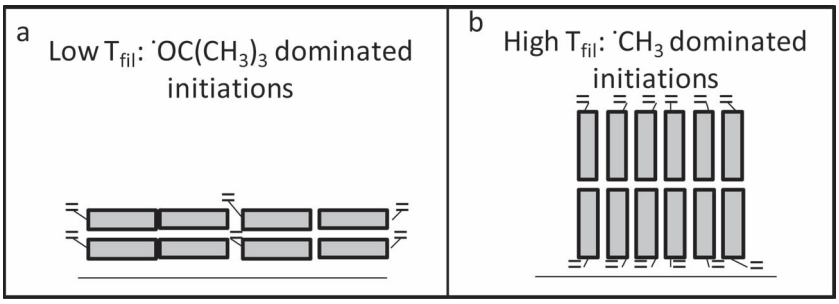

Scheme 4. Shift in the preferred crystallographic orientation of the chains from perpendicular to parallel to the substrate surface depending on the filament temperature. At low filament temperature the initiation is dominated by the tert-butoxy radicals, which preferentially drive the chains to be oriented parallel to the substrate. At high filament temperature the initiation is dominated by methyl radicals, which allow a vertical alignment of the chains.

the dramatic change in intensity between these two orientations strongly supports the hypothesis that at low T_{fil}, the perfluoro side groups are mostly aligned parallel to the substrate while they adopt a perpendicular orientation at high T_{fil}. Thus, changing filament temperature does not result in a transition between the amorphous and crystalline phases, but rather a shift in the preferred crystallographic orientation of the chains from perpendicular to parallel to the substrate surface, as shown in Scheme 4.

We hypothesize that the observed change in crystal texture results from the different initiator radicals dominating in the different T_{fil} regimes. In a lamellar bilayer structure, the vinyl bonds are not easily accessible. Therefore, the smaller methyl radicals created at higher filament temperature can more readily penetrate this structure and allow a vertical alignment of the perfluoro side chains. At low filament temperature, initiation by the bulky tert-butoxy radicals dominates and occurs more readily when vinyl bonds are exposed by orienting the perfluoro side chains horizontal to the substrate.

AFM morphological analysis for the samples deposited at different filament temperatures is shown in **Figure 6**. Figure 6a,b show the topographical images of the samples deposited at 240 °C and 300 °C, respectively. Also in this case, some aggregates are easily detectable on both surfaces. The size and number of the aggregates increase with the filament temperature, causing the RMS roughness to increase from 23 nm to 60 nm, as shown in Figure 6c. It is important to notice that the texture in which the chains are oriented parallel to the substrate does not induce as strong of a surface roughening as the fiber-like texture, which is characterized by RMS roughness values higher than 40 nm. This can be very advantageous for applications in which relatively smooth but still crystalline films are needed.

Finally, **Figure 7** shows the dynamic WCA as a function of the filament temperature. The advancing angles increase with the filament temperature from 132° to 150°. On the contrary, the receding contact angles decrease from 124° to 108°, causing an increase of the hysteresis from 7 to 40°. Since the polymers show semicrystalline organization for almost all the conditions explored in these experiments, it is expected that the chain reorganization is minimized for all the conditions, while the morphology may be the most important factor in this case. It is well known in the literature that a "properly configured" surface morphology may cause a passage from a Wenzel[21] (sticky hydrophobicity with high hysteresis) to a Cassie–Baxter[22] regime (slippery hydrophobicity when low hysteresis is measured).

A certain slippery behavior is observed for the samples deposited at low filament temperature, characterized by an advancing WCA of 132° and hysteresis of 7°. Increasing the filament temperature, the advancing WCA increases to 150° but a large hysteresis is also detected (40°), defining more a sticky regime. Apparently the fiber-like texture that is formed at higher filament temperature induces the formation of a morphology that enhances the hydrophobicity of the coating but probably the spacing of the aggregates formed on the surface is high related to their depth and therefore water is allowed to fill the gaps and sticks on the surface.

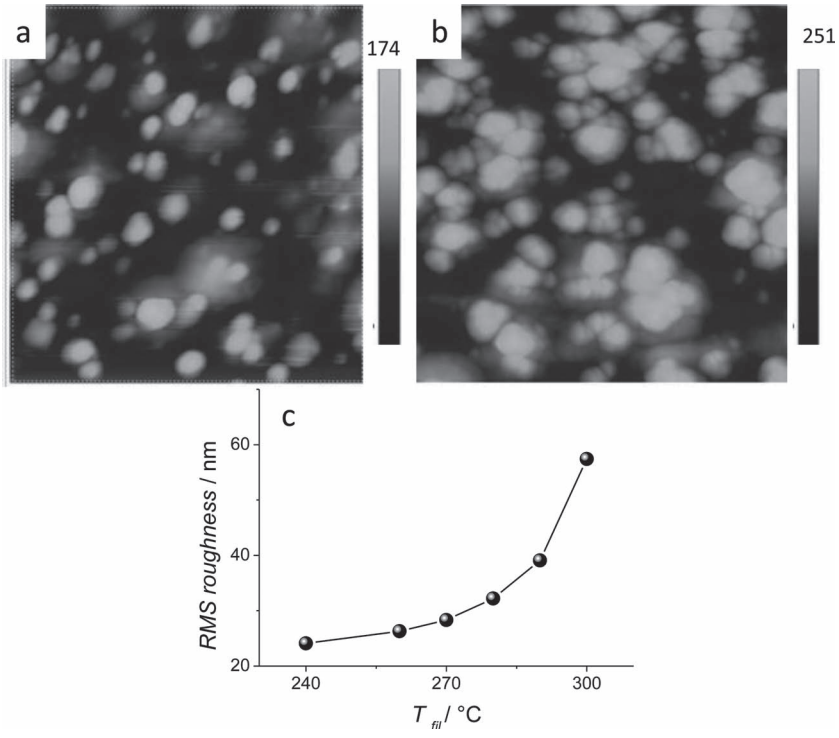

Figure 6. Topographical AFM images of the samples deposited at a) T_{fil} = 240 °C and b) T_{fil} = 300 °C. The size of the islands increases with the filament temperature. c) RMS roughness data plot as a function of T_{fil}. The roughest films are obtained at high temperature.

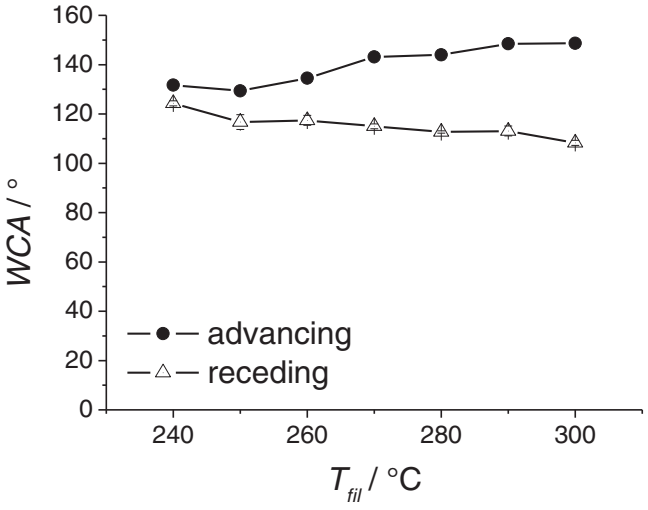

Figure 7. Advancing and receding WCAs measured for the coating deposited at different filament temperature. At high filament temperature the hysteresis increases while at low filament temperature hysteresis as low as 9° can be obtained.

2.3. Substrate Temperature

Because the chain growth and polymerization reactions in iCVD processes happen at the surface,[13,14] another parameter that can greatly influence the molecular organization is the substrate temperature. This section describes the changes in crystallinity and morphology obtained by changing T_{sub} (experimental conditions reported in Table 1).

Figure 8 shows the diffraction pattern and morphological results obtained varying the substrate temperature. The XRD profiles for the coating deposited at substrate temperatures of 30 and 45 °C are shown in Figure 8a. The XRD pattern remains the same for the two temperatures but the intensities increase at lower substrate temperature. The only peaks that are detected when irradiating the sample at 0° are the ones of the bilayer structure at small angle, demonstrating a fiber-like texture. The peaks for the sample deposited at 45 °C are broad while the peak intensity increases at lower temperature. This may be due to an enhancement of the crystallinity from a predominantly amorphous phase to a semicrystalline one. Topographical AFM images of the samples deposited at T_{sub} = 45 °C and 30 °C are shown, respectively, in Figure 8b and c. The number of particles detected and their size increase when the substrate temperature is decreased, correspondingly the RMS roughness slightly increases from 29 to 33 nm. As a result, at lower substrate temperature the crystallinity is enhanced and this causes the formation of more aggregates on the sample surface, as observed also in the other sets of experiments.

Further decreasing the substrate temperature caused the removal of portions of the fluorinated polymers from the silicon substrate. Scanning electron microscopy (SEM) (Figure 8d,e) and AFM (Figure 8f) images of the surface obtained for the sample deposited at 20 °C show this phenomenon. Figure 8e shows the elemental analysis made with the back scattering electron detector, and it clearly shows that the fractal structure observed in Figure 8e is a hole. The same is confirmed by the AFM analysis (Figure 8f) that shows an average vertical distance between the dark region and the bright region of 287 nm, which is almost the entire coating thickness. Due to regularity of the fractal profile of the missing coating it is reasonable to assume that the entire crystallite desorbs when the sample is deposited at 20 °C. This phenomenon can be ascribed to the low surface energy of the fluorinated coating, which results in bad adhesion with the silicon wafer surface as is very often observed for crystalline thin films deposited on non-wetting substrates.[30] The retracting of the polymer so as to minimize the interface with the substrate is therefore energetically favored. Higher surface temperatures allow one to avoid this kind of partial surface dewetting due to the enhancement of the surface reactions. Poly et al.[31] observed the same phenomenon when annealing a linear fluorinated polymer and found that the introduction of cross-links enables a strong inhibition of this phenomenon but also the loss of organization of the pendant fluorinated chains due to limitation of accessible conformations induced by cross-links and therefore of the crystallinity. Instead, in this case the phenomenon can be avoided by increasing the temperature (to 30 °C) without losing the crystallinity. Another reason for the removal of a portion of the coating may be the presence of

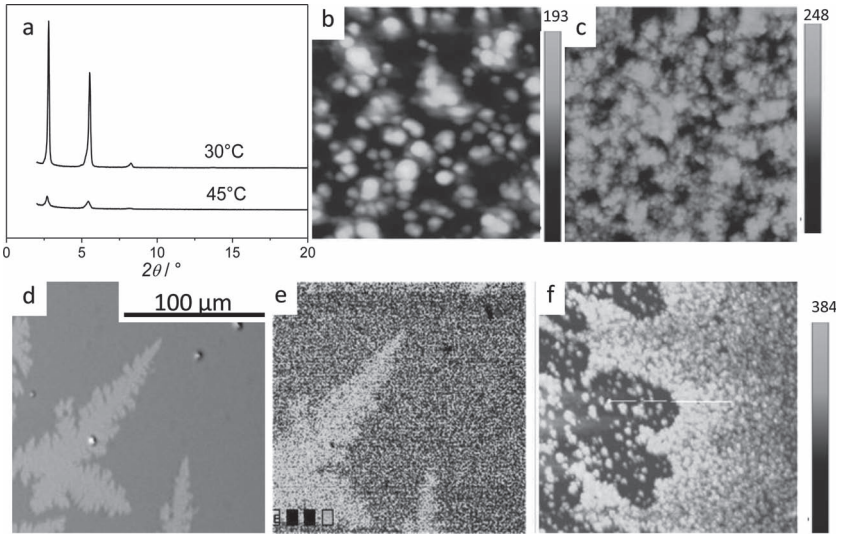

Figure 8. a) XRD profiles for the coating deposited at substrate temperatures of 30 and 45 °C when the sample is oriented perpendicular to the beam (0°). The XRD peaks sharpen at lower substrate *T*. Topographical AFM images of the samples deposited at T_{sub} = 45 °C (b) and 30 °C (c). The roughest surface is the one of the coating deposited at lower *T* where the crystalline phase is predominant. SEM (d,e) and AFM (f) images of the surface obtained for the sample deposited at 20 °C showing the removal of part of the coating from silicon substrate. Panel (e) shows the elemental analysis made with the back scattering electron detector. F and C are shown as dark grey and Si as light grey. The average vertical distance between the dark region and the bright region in (f) is 287 nm, which is almost the entire coating thickness.

unreacted monomer or short I–M–I chains that are volatile and delaminate from the surface after the deposition. As observed for other iCVD coatings, this generally creates a hole with a round shape.[32] In this case the observed shape is a fractal due to the crystallinity of the polymer.

3. Conclusions

In the present work we explored the formation of texturing in p-PFDA coatings deposited by iCVD. The results obtained clearly established a direct relationship between the organization of the fluorinated side chains inside smectic phases and the surface properties of the coatings prepared with the various polymers. The demonstration of texturing in these films may be very useful for some applications where a certain anisotropy is needed. Moreover, as demonstrated, it allows one to obtain higher hydrophobicity with lower surface reconstruction compared to amorphous polymers.

Changing the deposition conditions, the chemical bonding environment of the coatings remained largely unchanged. On the other hand, the molecular organization of the chains and sidegroups was significantly affected by the external conditions, such as initiator to monomer flow rate ratio, filament temperature, and substrate temperature.

Using a large initiator to monomer flow rate ratio drives the transition from a semicrystalline to amorphous phase with a maximum of crystallinity index at around I/M = 4. Moreover at I/M = 3–4 the surface properties were also the most stable, in fact the WCA hysteresis was as low as 9°: the high crystallinity hinders large surface reconstruction. This has been also confirmed by angle-resolved XPS experiments, which showed a large CF_3 component also in depth. At high I/M ratios, in which the amorphous components are predominant, the CF_3 component is weak in depth and increases towards the surface. The morphology was also significantly affected by the transition from the crystalline to the amorphous phase, in fact the RMS roughness decreased from 40 to 10 nm.

Changing the filament temperature instead provoked a change in the orientation of the chains: at high filament temperature a fiber-like texture was detected, while at low T_{fil} the chains were oriented mostly parallel to the substrate. This was speculated to be a consequence of the change on the initiator radical that initiates the polymerization process: at higher temperature methyl radicals are formed by β-scission of the tert-butoxy radicals. Methyl radicals are less bulky than tert-butoxy ones therefore they allow the formation of a vertical alignment of the chains. The film deposited at low filament temperature showed the lowest RMS roughness and also the lowest WCA hysteresis. The horizontal alignment of the chains can be favorable for applications where low surface energy, flatness, and stable surface properties are needed.

Finally, another important aspect of this paper is that we demonstrated that by tuning the deposition conditions we can take control over the process of morphology formation induced by crystallization. Indeed the crystalline domains spontaneously aggregate, resulting in large particle formation (radius higher than 100 nm) on the surface but this can be limited using low initiator flow rates or low filament temperatures. It is important to notice that the texture in which the chains are oriented parallel to the substrate does not induce as strong of a surface roughening as the fiber-like texture, which is characterized by RMS roughness values higher than 40 nm. This can be very advantageous for applications in which relatively smooth but still crystalline films are needed, while fiber-like texturing can be useful for applications where rough surfaces are preferable, e.g., biomaterials.

4. Experimental Section

The deposition chamber was a custom-built cylindrical vacuum reactor. The chamber was 24.6 cm in diameter and 3.8 cm in height. The reactor had a removable quartz top (2.5 cm thick) to allow visual inspection and laser interferometry. The reactor was pumped by a mechanical Fomblin pump (Leybold, Trivac) and the pressure was monitored with a MKS capacitive gauge.

The liquid monomer (PFDA, 97% Aldrich) and initiator (TBPO, 98% Aldrich) were used without any further purification steps. The monomer was vaporized, maintaining the liquid jar at 80 °C and was then introduced into the reactor through a needle valve. The initiator was kept at room temperature and introduced through a mass flow controller (MKS Instrument). The labile peroxide bond of the initiator was thermally broken by a filament array of 14 parallel nickel chromium filaments (Goodfellow) at a distance of 1.5 cm from the substrate. The filaments were heated to temperatures in the range of 250–300 °C using a DC power supply (Sorensen). T_{fil} and T_{sub} were monitored by two thermocouples (Type K, Omega Engineering). The substrate temperature was adjusted (with an error of ±2 °C) using a chiller/heater (NESLAB). The film growth was monitored in real-time by reflecting a He-Ne laser (JDS Uniphase) off the substrate and the film and recording the interference laser signal intensity as a function of time. Each film was deposited up to a thickness of 300 ± 10 nm.

Three sets of experiments were performed, as shown in Table 1) changing the flow rate ratio of initiator to monomer in the range of 0.5–6, 2) changing the filament temperature (250–300 °C), and 3) changing the substrate temperature from 20–50 °C. For the first set of experiments a total flow rate of 5.2 sccm was maintained by using a patch flow of nitrogen in order to keep the residence time of the active species in the reactor chamber constant.

The chemical characterization of the films was performed by FTIR spectroscopy using a Nexus 870 FTIR, Thermo Nicolet spectrometer equipped with a deuterated triglycine sulfate (DTGS)-thermoelectrically cooled (TEC) detector in transmission mode. The spectra were acquired from 4000 to 400 cm^{-1} with a resolution of 4 cm^{-1} repeating 256 scans. The spectrum of a bare Si wafer was used as the background. In order to minimize the effects of water vapor and carbon dioxide absorption, the spectrometer was purged with nitrogen for 15 min between each measurement.

The film thicknesses were measured by ex situ variable angle spectroscopy ellipsometry (VASE, JA Woollam M-2000). The measurements were done at three different angles (65°, 70°, and 75°) in the wavelength range of 200–1000 nm. The applied optical model consisted of three components: the silicon substrate, the native SiO_2 layer of 1.7 nm, and the film bulk layer. The bulk components were modeled by the Cauchy function adding the Urbach tail to model the absorption.

The elemental analysis was done using ARXPS. The XPS spectra were obtained using a SSX-100 X-probe (Surface Science Instruments) spectrometer equipped with a monochromatized Al K_α source, operated at 1486.8 eV. Survey scans were conducted at take-off angles of 0°, 30°, and 70° with the surface normal to sample the surface at different penetration depths. During the XPS analysis, the sample charge was compensated by a 1 eV electron beam at high neutralization current by means of a flood gun. The pass energy was 150 V for survey scans and 50 V for high-resolution scans. The pressure during analysis was kept

under 2×10^{-9} Torr. A 1 mm diameter beam was used in the analysis. CasaXPS software was used to fit the high-resolution spectra. Samples were stored under vacuum overnight prior to analysis.

Surface film morphology was investigated by AFM (Digital Instruments, D3100-1). Images were acquired in tapping mode using conical gold-coated silicon tips. RMS roughness was measured on 5×5 μm^2 surface areas.

Deposited trench wafers were sputter-coated with 6 nm of gold (Denton Desk V) and images were obtained by SEM (Hitachi, TM 3000) with an acceleration voltage of 15 kV. In some cases the images were also acquired using the Energy dispersive x-ray spectrometer (EDS) mode to detect the back scattered electron (BSE) and have an elemental map. In this case the working distance was set at 8.5 mm from the detector.

WCA were measured using a goniometer equipped with an automated dispenser (Model 500, Rame-Hart). Advancing and receding angles were measured with the sessile drop method by depositing a droplet of 1 μL on the surface, then increasing the volume to 4 μL, and finally decreasing it. Advancing angles were considered as the maximum angles observed during the droplet growth. Receding contact angles were measured in correspondence with the drop profile just before the contact surface reduction. Each WCA value was averaged from measurements of four drops with an estimated maximum error of 4°.

The crystalline states of the p-PFDA thin films was determined by XRD. The XRD measurements were carried out on a Scintag θ–θ diffractometer with a Cu K-alpha radiation (1.541867 Å) at 40 kV and 44 mA. Data was collected in continuous mode at 3° min^{-1}, with a step size of 0.02°. The scans were taken in symmetrical reflection geometry. A non-linear least-squares regression was performed on the diffraction peak at 2.8° using two Lorentz components using the "Fit multi-peaks" procedure of the OriginLab software.

Supporting Information

Supporting Information is available from the Wiley Online Library or from the author.

Acknowledgements

The authors acknowledge financial support from the MIT Institute for Soldier Nanotechnologies (ISN) under Contract DAAD-19-02D-0002 with the U.S. Army Research Office.

Received: December 15, 2011
Published online: February 23, 2012

[1] A. Curtis, C. Wilkinson, *Trends Biotechnol.* **2001**, *19*, 97.
[2] C. D. W. Wilkinson, M. Riehle, M. Wood, J. Gallagher, A. S. G. Curtis, *Mater. Sci. Eng. C* **2002**, *19*, 263.
[3] D. L. Schmidt Jr., R. F. Brady, K. Lam, D. C. Schmidt, M. K. Chaudhury, *Langmuir* **2004**, *20*, 2830.
[4] R. Blossey, *Nat. Mater.* **2003**, *2*, 301.
[5] M. Gupta, K. K. Gleason, *Langmuir* **2006**, 10047.
[6] S. R. Coulson, I. S. Woodward, J. P. S. Badyal, S. A. Brewer, C. Willis, *Langmuir* **2000**, *16*, 6287.
[7] K. Honda, M. Morita, H. Otsuka, A. Takahara, *Macromolecules* **2005**, *38*, 5699.
[8] V. V. Volkov, N. A. Platè, A. Takahara, T. Kajiyama, N. Amaya, Y. Murata, *Polymer* **1992**, *33*, 1316.
[9] A. Takahara, N. Morotomi, S. Hiraoka, N. Higashi, T. Kunitake, T. Kajiyama, *Macromolecules* **1989**, *22*, 617.
[10] T. D. Hadnagy, *Integr. Ferroelectr.* **1997**, *18*, 1.
[11] A. G. Pittman, B. A. Ludwig, *J. Polym Sci. A* **1969**, *7*, 3053.
[12] A. Milella, R. DiMundo, F. Palumbo, P. Favia, F. Fracassi, R. d'Agostino, *Plasma Process. Polym.* **2009**, *6*, 460.
[13] K. K. S. Lau, K. K. Gleason, *Macromolecules* **2006**, *39*, 3695.
[14] K. K. S. Lau, K. K. Gleason, *Macromolecules* **2006**, *39*, 3688.
[15] G. Ozaydin-Ince, K. K. Gleason, *J. Vac. Sci. Technol. A* **2009**, *27*, 1135.
[16] G. Ozaydin-Ince, K. K. Gleason, *Chem. Vap. Deposition* **2010**, *16*, 100.
[17] N. S. Murthy, H. Minor, *Polymer* **1990**, *31*, 996.
[18] Y. Mao, K. K. Gleason, *Langmuir* **2004**, *20*, 2484.
[19] A. K. H. Achyuta, A. J. White, H. G. Pryce Lewis, S. K. Murthy, *Macromolecules* **2009**, *42*, 1970.
[20] A. M. Coclite, G. Ozaydin-Ince, R. d'Agostino, K. K. Gleason, *Macromolecules* **2009**, *42*, 8138.
[21] R. W. Wenzel, *Ind. Eng. Chem.* **1936**, *28*, 988.
[22] A. B. D. Cassie, S. Baxter, *Trans. Faraday Soc.* **1944**, *40*, 546.
[23] S. Tanuma, C. J. Powell, D. R. Penn, *Surf. Interface Anal.* **1993**, *21*, 165.
[24] G. Beamson, D. Briggs, *High resolution XPS of Organic Polymers, The Scienta ESCA300 Database*, Wiley, Chichester **1992**.
[25] Y. Mao, K. K. Gleason, *Macromolecules* **2006**, *39*, 3895.
[26] D. L. Schmidt, C. E. Coburn, B. M. Dekoven, G. E. Potter, G. F. Meyers, D. A. Fischer, *Nature* **1994**, *368*, 39.
[27] M. Strobel, C. S. Lyons, *Plasma Process. Polym.* **2011**, *8*, 8.
[28] R. DiMundo, F. Palumbo, *Plasma Process. Polym.* **2011**, *8*, 14.
[29] P. G. Mekarbane, B. J. Tabner, *Macromolecules* **1999**, *32*, 3620.
[30] M. Ramanathan, S. B. Darling, *Prog. Polym. Sci.* **2011**, *36*, 793.
[31] J. Poly, E. Ibarboure, J. Rodriguez-Hernandez, D. Taton, E. Papon, *Macromolecules* **2010**, *43*, 1299.
[32] A. M. Coclite, K. K. Gleason, *Plasma Process. Polym.* DOI: 10.1002/ppap.201100167.